

# Polarized Scattering and Biosignatures in Exoplanetary Atmospheres

S.V. Berdyugina<sup>1</sup>

E-mail: *berdyugina@kis.uni-freiburg.de*

Polarized scattering in planetary atmospheres is computed in the context of exoplanets. The problem of polarized radiative transfer is solved for a general case of absorption and scattering, while Rayleigh and Mie polarized scattering are considered as most relevant examples. We show that (1) relative contributions of single and multiple scattering depend on the stellar irradiation and opacities in the planetary atmosphere; (2) cloud (particle) physical parameters can be deduced from the wavelength-dependent measurements of the continuum polarization and from a differential analysis of molecular band absorption; (3) polarized scattering in molecular bands increases the reliability of their detections in exoplanets; (4) photosynthetic life can be detected on other planets in visible polarized spectra with high sensitivity. These examples demonstrate the power of spectropolarimetry for exoplanetary research and for searching for life in the universe.

## 1 Polarized Radiative Transfer

Radiative processes in planetary atmospheres is a classical subject, simply for the reason that we live in one. Extensive theoretical studies were carried out during the second half of the twentieth century by such giants as Sobolev [1] and Chandrasekhar [2] as well as the renown radiative transfer school at the Saint Petersburg (Leningrad) University [3]. Most recently, physics of planetary atmospheres has become one of the most acclaimed subjects because of applications for Earth climate studies and the detection of a large variety of extrasolar planets. This paper provides the theoretical basis for studying atmospheres of exoplanets using techniques of spectropolarimetry available to us. In particular, using molecular band and continuum spectropolarimetry one can reveal the composition of the gaseous atmosphere, particle layers (clouds, hazes, etc.) and the planetary surface, including the land, water, and life. Modeling these cases is described in this paper.

We start from solving a self-consistent radiative transfer problem for polarized scattering in a planetary atmosphere illuminated by a host star. We solve this problem under the following assumptions: 1) the atmosphere is plane-parallel and static; 2) the planet is spherically symmetric; 3) stellar radiation can enter the planetary atmosphere from different angles and can be polarized; 4) an incoming photon is either absorbed or scattered according to opacities in the atmosphere; 5) an absorbed photon does not alter the atmosphere (model atmosphere includes thermodynamics effects of irradiation); 6) photons can be scattered multiple times until they escape the atmosphere. These assumptions expand those in [4], namely that multiple scattering is allowed, stellar irradiation can be polarized and vary with an incident angle, and the planetary atmosphere can be inhomogeneous in both longitude and latitude.

Then, the radiative transfer equation for the Stokes vector  $\mathbf{I} = (I, Q, U, V)^T$  of scattered polarized radiation of a given frequency (omitted for clarity) towards  $(\mu = \cos \theta, \varphi)$  is

$$\mu \frac{d\mathbf{I}(\tau, \mu, \varphi)}{d\tau} = \mathbf{I}(\tau, \mu, \varphi) - \mathbf{S}(\tau, \mu, \varphi) \quad (1)$$

with the total source function

$$\mathbf{S}(\tau, \mu, \varphi) = \frac{\kappa(\tau)\mathbf{B}(\tau) + \sigma(\tau)\mathbf{S}_{sc}(\tau, \mu, \varphi)}{\kappa(\tau) + \sigma(\tau)}, \quad (2)$$

---

<sup>1</sup> Kiepenheuer Institut für Sonnenphysik, Freiburg, Germany

where  $\kappa$  and  $\sigma$  are absorption and scattering opacities,  $\mathbf{S}_{\text{sc}}$  and  $\mathbf{B}$  are the scattering source function and the unpolarized thermal emission, respectively, and  $\tau$  is the optical depth in the atmosphere with  $\tau = 0$  at the top. The formal solution of Eq. (1) is (e.g., [1])

$$\mathbf{I}(\tau, \mu, \varphi) = \mathbf{I}(\tau_*, \mu, \varphi) e^{-(\tau_* - \tau)/\mu} + \int_{\tau}^{\tau_*} \mathbf{S}(\tau', \mu, \varphi) e^{-(\tau' - \tau)/\mu} \frac{d\tau'}{\mu}, \quad (3)$$

where  $\tau_*$  is either the optical depth at the bottom of the atmosphere for the Stokes vector  $\mathbf{I}^+(\tau, \mu, \varphi)$  coming from the bottom to the top ( $\theta < \pi/2$ ) or the optical depth at the top of the atmosphere ( $\tau_* = 0$ ) for the Stokes vector  $\mathbf{I}^-(\tau, \mu, \varphi)$  coming from the top to the bottom ( $\theta > \pi/2$ ).

The scattering source function  $\mathbf{S}_{\text{sc}}$  is expressed via the scattering phase matrix  $\hat{\mathbf{P}}(\mu, \mu'; \varphi, \varphi')$ , depending on the directions of the incident ( $\mu', \varphi'$ ) and scattered ( $\mu, \varphi$ ) light:

$$\mathbf{S}_{\text{sc}}(\tau, \mu, \varphi) = \int \hat{\mathbf{P}}(\mu, \mu'; \varphi, \varphi') \mathbf{I}(\tau, \mu', \varphi') \frac{d\Omega'}{4\pi}. \quad (4)$$

It has contributions from scattering both incident stellar light and intrinsic thermal emission. Their relative contributions depend on the frequency. For instance, for Rayleigh scattering the intensity of the thermal emission of a relatively cold planet in the blue part of the spectrum may become negligible compared to that of the scattered stellar light. The phase matrix  $\hat{\mathbf{P}}(\mu, \mu'; \varphi, \varphi')$  is a  $4 \times 4$  matrix with six independent parameters for scattering cases on particles with a symmetry [5]. In this paper we employ the Rayleigh and Mie scattering phase matrices but our formalism is valid for other phase functions too.

The Stokes vector of the light emerging from the planetary atmosphere  $\mathbf{I}(0, \mu, \varphi)$  is obtained by integrating iteratively Equations (2) and (3) for a given vertical distribution of the temperature and opacity in a planetary atmosphere. Boundary conditions are defined by stellar irradiation at the top, planetary thermal radiation at the bottom, and (if present) reflection from the planetary surface. Stellar irradiation can be polarized, but the planetary thermal radiation is unpolarized. In particular, stellar limb darkening and linear polarization due to scattering in the stellar atmosphere [7, 8] can be taken into account, including the influence of dark spots on the stellar surface [9]. This effect is not very large but may be important for cooler stars with large spots and planets on very short-period orbits (when the stellar radiation incident angle noticeably vary depending on the stellar limb angle). Also, stellar magnetic fields causing polarization in stellar line profiles due to the Zeeman effect can be included for given atomic and molecular lines [17]. This effect is only important for high-resolution spectropolarimetry which is not yet possible for exoplanets. Depending on the structure of the phase matrix and the boundary conditions, the equations are solved for all or a fewer Stokes vector components. Normally it takes 3–7 iterations to achieve a required accuracy. The radiation flux is then obtained by integrating the Stokes vector over the illuminated planetary surface with a coordinate grid ( $6^\circ \times 6^\circ$ ) on the planetary surface for a given orbital phase angle as described in [4].

Our model includes the following opacity sources: (1) Rayleigh scattering on H I, H<sub>2</sub>, He I, H<sub>2</sub>O, CO, CH<sub>4</sub> and other relevant molecules, Thomson scattering on electrons, and Mie scattering on spherical particles with a given size distribution, with all scattering species contributing to the continuum polarization, (2) absorption in the continuum due to free-free and bound-free transitions of H I, He I, H<sup>-</sup>, H<sub>2</sub><sup>+</sup>, H<sub>2</sub><sup>-</sup>, He<sup>-</sup>, metal ionization, and collision-induced absorption (CIA) by H<sub>2</sub>–H<sub>2</sub>; (3) absorption and scattering in atomic and molecular lines for particular frequencies where they contribute. Number densities of the relevant species are calculated with a chemical equilibrium code described in [17]. Here we employ model atmospheres from [10] and [11] for stellar and planetary atmospheres, respectively, according to their effective temperatures ( $T_{\text{eff}}$ ). This is appropriate for illustrating radiative transfer effects discussed in Section 2 and applicable for the case of highly irradiated hot Jupiters and substellar components. In particular, a model atmosphere of a hot Jupiter has to match the infrared thermal radiation of the planet originating in deeper layers, while upper layers contributing to the optical radiation are completely dominated by the incident stellar radiation. Planetary atmosphere models with specific chemical compositions and temperature-pressure (TP) structures can be also employed. For instance,

the planetary atmosphere can be inhomogeneous with the vertical composition and TP-structure varying with latitude and longitude.

## 2 Results

### 2.1 Rayleigh Scattering

In this section we assume that scattering in the planetary atmospheres occurs only on atoms, molecules or particles which are significantly smaller than the wavelength of scattered light, i.e., we employ the Rayleigh scattering phase matrix, including isotropic scattering intensity. In particular, we focus here on examples of resulting Stokes parameters and source functions depending on stellar irradiation and wavelength.

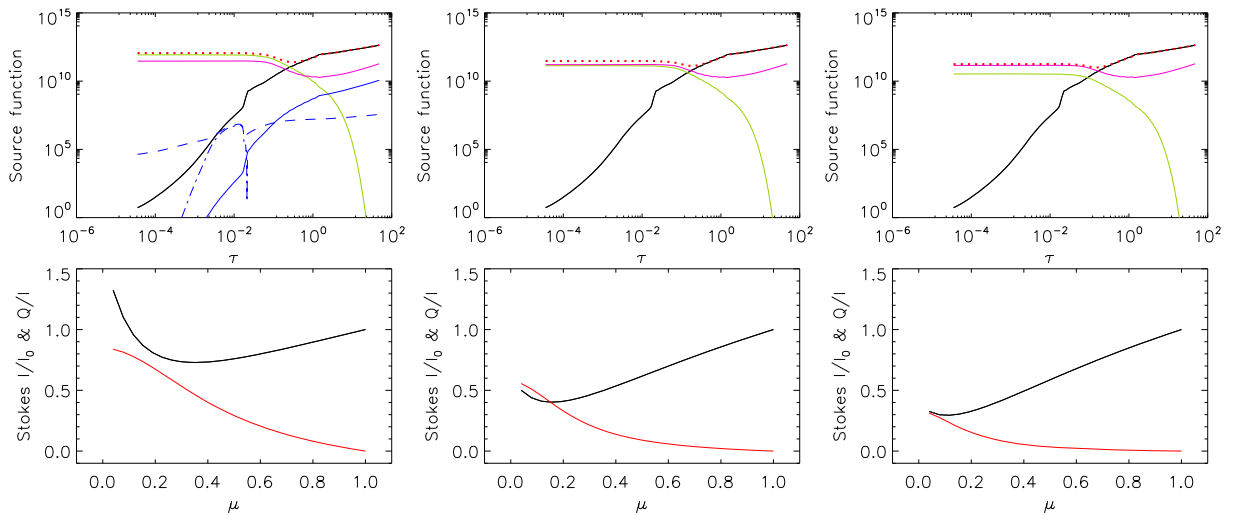


Figure 1: Stokes  $I$  source functions (top panels) and normalized emerging Stokes  $I$  and  $Q$  parameters (bottom panels) for three distances between the star and the planet: 0.02, 0.05, and 0.1 AU (left to right). The source functions are shown separately for thermal radiation of the planet (black), single scattered stellar radiation (green), multiple scattered stellar and planetary radiation (magenta), and the total one (red dotted line). The top left plot also shows relative scattering (dashed blue) and absorption (solid blue) opacities and separately particle scattering (dashed-dotted blue) as a cloud layer in the original model atmosphere (it is the same for all three panels). In the lower panels, the Stokes  $I/I_0$  (black) is normalized to the intensity at the planet disk centre ( $\mu = 0$ ). The Stokes  $Q/I$  (red) is normalized to  $I$  at given  $\mu$ . Both are at  $\tau = 0$ . Notice the increase of the single scattering contribution with respect to that of multiple scattering as the the distance to the planet decreases (i.e., the stellar flux increases). Accordingly, the planet limb polarization and brightening increase too.

Figure 1 shows examples of depth dependent Stokes  $I$  source functions (top panels) and normalized emerging Stokes  $I$  and  $Q$  (bottom panels) for three distances between the star and the planet (left to right) at the wavelength of 400nm. Here, the star is of  $T_{\text{eff}} = 5500$  K, and the planet is of  $T_{\text{eff}} = 1500$  K. Stokes  $Q$  is assumed to be positive when polarization is perpendicular to the scattering plane. By studying the behaviour of the source functions and Stokes parameters depending on various parameters we conclude the following facts:

- The polarization at a given depth in the atmosphere arises due to its anisotropic irradiation, i.e., unequal illumination coming from the top and from the bottom (assuming here an azimuthal symmetry). Hence, anisotropy and polarization are small in deeper layers, where planet thermal radiation dominates, and they are larger in upper layers, where stellar irradiation dominates. The

depth where this dominance alternates depends on the relative contribution of the scattering and absorption coefficients to the total opacity (which is wavelength dependent). It turns out that in cool gaseous atmospheres this occurs very deep in the atmosphere for the continuum radiation, but can be higher for radiation in cores of strong absorption atomic and molecular lines.

- This anisotropy (and, hence, polarization) is sensitive to the incident stellar flux (cf., number of photons arriving to the planet) at wavelengths where Rayleigh scattering is most efficient, i.e., in the blue part of the spectrum. Thus, hotter stars hosting closer-in planets are systems potentially producing larger polarization in the blue.
- Relative contribution of single-scattered photons with larger polarization with respect to multiple-scattered photons with lower resulting polarization increases with stellar irradiation at shorter wavelengths.
- Depending on stellar irradiation, intensity distribution on the planetary disk, i.e.,  $I(0, \mu)/I(0, 1)$  can decrease or increase with  $\mu$ . In fact, the  $\mu$  value where limb darkening turns into limb brightening approximates the optical depth  $\tau$  where single and multiple scattering contributions become comparable.
- Planet limb polarization is very sensitive to the stellar irradiation because of the effects listed above. For a larger stellar flux, a larger polarization is seen for a wider range of angles.
- Considering the high sensitivity of planet polarization to stellar irradiation, variability of the stellar flux incident on the planet, e.g., caused by dark (magnetic) spots or flares, can result in a variable *amplitude* of planet polarization, while its orbital phase dependence is preserved, since the latter depends on orbital parameters only (see [4]).

The models presented in Figure 1 are close to the case of the HD189733b hot Jupiter which is at about 0.03 AU from its K-dwarf star with the effective temperature of about 5500 K. The relatively high polarization measured from this planet in the blue band (B-band) [12, 13] is well explained by the dominance of the single-scattered stellar photons in its upper atmosphere because of the high irradiation and Rayleigh scattering cross-section in the blue. This was first proposed in [13] and further demonstrated with a simple model in [14]. Here, with the precise calculations of the polarized radiative transfer, we show that this hypothesis is valid. Moreover, multi-wavelength polarimetry allowed for estimating the planet albedo and determining its blue colour. The relation between the geometrical albedo and polarization is however not so simple as was assumed in [13]. An analysis of this relation for various planetary and stellar parameters using this theory will be carried out in a separate paper.

## 2.2 Mie Scattering

In this section we consider scattering caused by spherical particles of various sizes which can be comparable or larger than the wavelength of scattered light, i.e., we employ the Mie scattering phase matrix. For smaller particles and/or longer wavelengths it approximates Rayleigh scattering.

Following examples in earlier literature (e.g., [5] and references therein), we assume "gamma" distribution of particle sizes:  $n(r) = Cr^{(1-3b)/b}e^{-r/ab}$ , with  $a$  and  $b$  being the effective particle radius and the effective size variance, respectively. Also, we use the so-called size parameter  $2\pi a/\lambda$  which can be recalculated to  $\lambda$  for a given  $a$ , and vice versa. Particles are characterized by the refractive index  $n_r$  with its real part being responsible for scattering. With this, we can reproduce numerical examples in [5] as well as results for Venus in [15]. Here, we investigate scattering on highly refractive materials ( $n_r > 1.5$ ) which are expected to be present in hot Jupiter atmospheres. For instance, olivine, which is common in the Solar system, and its endmembers forsterite  $Mg_2SiO_4$  and fayalite  $Fe_2SiO_4$  have a range of the refractive index from 1.6 to 1.9.

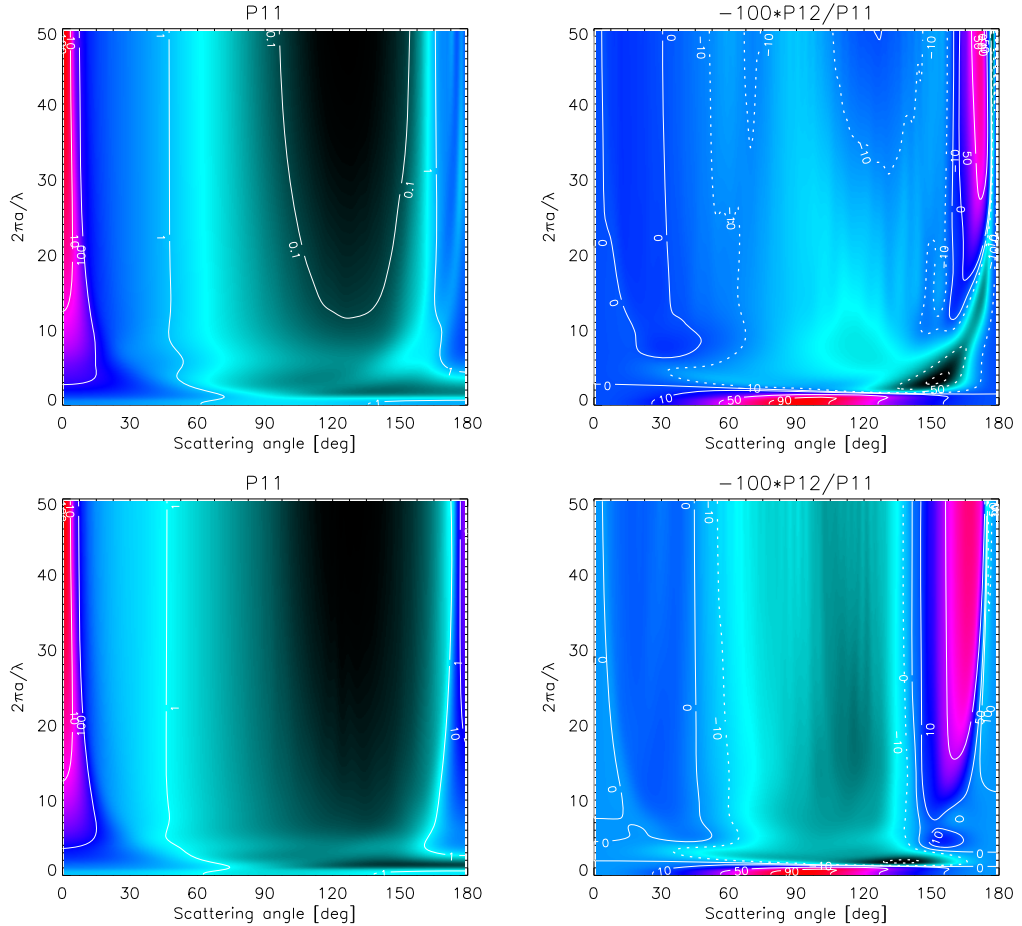


Figure 2: Mie scattering phase matrix elements  $P_{11}$  (intensity) and  $-100\%P_{21}/P_{11}$  (percent polarization) for single scattering on particles with  $n_r=1.6$  (top panels) and  $n_r=1.9$  (bottom panels) and the effective particle size variance  $b=0.07$ . Dotted lines are contours for negative polarization (parallel to the scattering plane).

In Fig. 2 we show examples of two Mie phase matrix elements: intensity  $P_{11}$  and percent polarization  $-100\%P_{21}/P_{11}$  for single scattering on particles with  $n_r$  of 1.6 (upper panels) and 1.9 (lower panels), depending on the size parameter and the scattering angle. The latter is  $0^\circ$  for forward and  $180^\circ$  for backward scattering. These examples illustrate the following known facts (e.g., [16, 15, 5]):

- Forward scattering dominates the intensity for larger particles.
- For the smallest particle size parameters polarization is strong (up to 100%) and positive near scattering angle  $90^\circ$  due to Rayleigh scattering. For the largest size parameters polarization approaches that of the geometrical optics, i.e., it is small at small scattering angles because of largely unpolarized diffracted light, and it is negative for a wide range of angles because of two refractions within a sphere.
- Strong positive polarization maximum near  $165^\circ$ – $170^\circ$  is the primary rainbow. It can reach 100% polarization for certain size-angle combinations.
- Strong negative polarization near  $140^\circ$ – $150^\circ$  is a "glory"-like phenomenon, caused by surface waves on the scattering particle. The "glory" itself, which is a sharp maximum in polarization in the backscattering direction, can be seen on particles with larger size parameters.

- Weak positive polarization near  $20^\circ$ – $30^\circ$  is due to "anomalous diffraction" caused by interference of the diffracted, reflected and transmitted light in the forward direction.

Now we can model effects of particle scattering on limb intensity and polarization distribution in planetary atmospheres by solving the polarized radiative transfer problem as described in Sect. 1 with the corresponding phase functions. As in Sect. 2.1, we investigate radiative transfer effects depending on irradiation and atmosphere properties. We use the same model atmospheres as before but replace the original layer of scattering particles in the planetary atmosphere with layers of various properties at different heights, imitating a variety of clouds. This *ad hoc* approach allows us to study intensity and polarization depending on particle (cloud) properties. Three examples are shown in Fig. 3. One can see that clouds can significantly affect the brightness of the irradiated atmosphere at depths (angles) where scattering and absorption opacities are comparable. In the presented example of the highly irradiated planetary atmosphere the polarization is still determined by the single-scattered stellar photons. In less irradiated atmospheres, the influence of particles is larger, but still according to the scattering and absorption profiles. More examples with a larger variety of clouds will be published elsewhere.

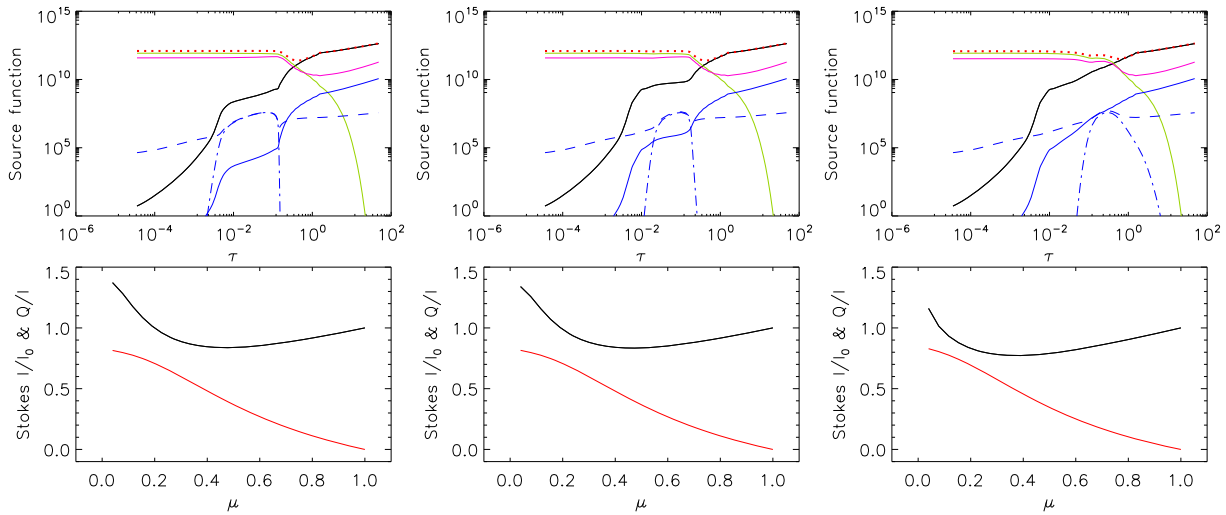


Figure 3: The same as Fig. 1 but for a planet at 0.02 AU from the star with an atmosphere containing *ad hoc* particle layers. The particles are assumed to have an effective size of 20nm, and the layers are at the depths of 70, 80, and 90 km from the top of the atmosphere (plots are from left to right, respectively).

### 2.3 Molecular Bands

Detecting molecular bands in planetary spectra is the key to their chemical composition and to their habitability assessment. By analysing the molecular composition we can establish whether the atmosphere is in equilibrium or it is affected by such non-equilibrium processes like stellar activity or life.

Including molecular bands into polarized radiative transfer requires computation of both line absorption and scattering coefficients. We compute molecular line absorption, following [17], and molecular line scattering, following [18], where magnetic field effects on molecular absorption and scattering (the Zeeman, Paschen-Back and Hanle effect) are also included and can be employed for exoplanets. These line opacities augment the continuum opacities at molecular band wavelengths. In addition, depending on the molecular number density distribution, the maximum absorption and scattering for different molecules and bands can occur at different heights [17]. This is an important diagnostics of the atmosphere thermodynamics, e.g., TP profiles.

Despite the growing amount of information, the molecular composition of exoplanetary atmospheres is still largely unknown. Several reported detections of molecular bands were disputed by later measurements

(e.g., see overview and references in [19]). Also, a few exoplanets were found to lack any spectral features in the near infrared which was interpreted as the presence of high clouds masking molecular absorption (e.g., [20]). To explain the presence or absence of molecular bands, synthetic flux absorption and emission thermal spectra in clear and cloudy planetary atmospheres were computed. Recently, it was proposed that cloud physical parameters can be constrained by a differential analysis of various molecular bands forming at different heights in the atmosphere with respect to the cloud height and extent [19]. For instance, water vapor bands at  $1.09 \mu\text{m}$  and  $1.9 \mu\text{m}$  show noticeably different sensitivity to particle size and cloud extent and position at intermediate depths in the atmosphere. This is a sensitive spectral diagnostics of clouds.

Polarized scattering in molecular bands was observed in the solar atmosphere and solar system planets (e.g., [18, 21]). To model this polarization we employ the radiative transfer theory described in Sect. 1 with the line scattering coefficient strongly dependent on wavelength (within line profiles), line polarizability and magnetic field (if included, via the Hanle effect) [18, 22]. The first order radiative transfer effect leads to an apparent correlation of line scattering with absorption. This effect increases the contrast of detection of weak signals in distant planets. For example, model spectra from [27] for the Earth atmosphere (Fig. 5, right panels) show polarization in molecular oxygen and water vapour bands in red wavelengths. However, because of the line-dependent polarizability and magnetic sensitivity, line polarization does not in general correlate with line absorption, as is observed in the Second solar spectrum [22]). Neglecting these effects impedes the quantitative interpretation of polarization and the inferred planet parameters. An example taking the polarizability effect into account for about 3500  $\text{H}_2\text{O}$  lines near  $1.4 \mu\text{m}$  is shown in Fig. 4.

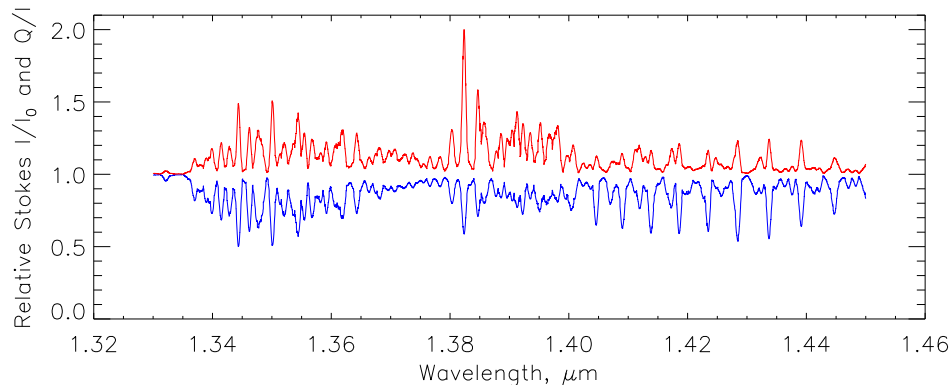


Figure 4:  $\text{H}_2\text{O}$  relative polarization (red) and absorption (blue) spectra plotted, respectively, up and down for clarity, taking into account line polarizability. Note that there is no exact correlation between polarization and absorption.

## 2.4 Biosignatures

A planetary surface visible through an optically thin atmosphere can be searched remotely for spectral and polarized imprints of organisms reflecting and absorbing stellar light. Due to the accessibility and amount of energy provided by the stellar radiation, it seems natural for life to evolve a photosynthetic ability to utilize it as an energy source also on other planets. Thus, flux spectral signatures of biological pigments arising from photosynthesis have been proposed as biosignatures on exoplanets [23, 24]. Moreover, it was recently shown that photosynthetic organisms absorbing visible stellar radiation with the help of various biopigments demonstrate a high degree of linear polarization associated with such absorption bands (see Fig. 5). This effect was also proposed as a sensitive biosignature for high-contrast remote sensing of life [25].

Capturing stellar energy by photosynthetic organisms relies on complex assemblies of biological

pigments. While chlorophyll *a* is the primary pigment in cyanobacteria, algae and plants, there are up to 200 accessory and secondary (synthesized) biopigments, including various forms of chlorophyll (*b*, *c* and *d*), carotenoids, anthocyanins, phycobiliproteins, etc [26]. Various spectral sensitivity of biopigments contribute to their ability to absorb almost all light in the visible range (Fig. 5).

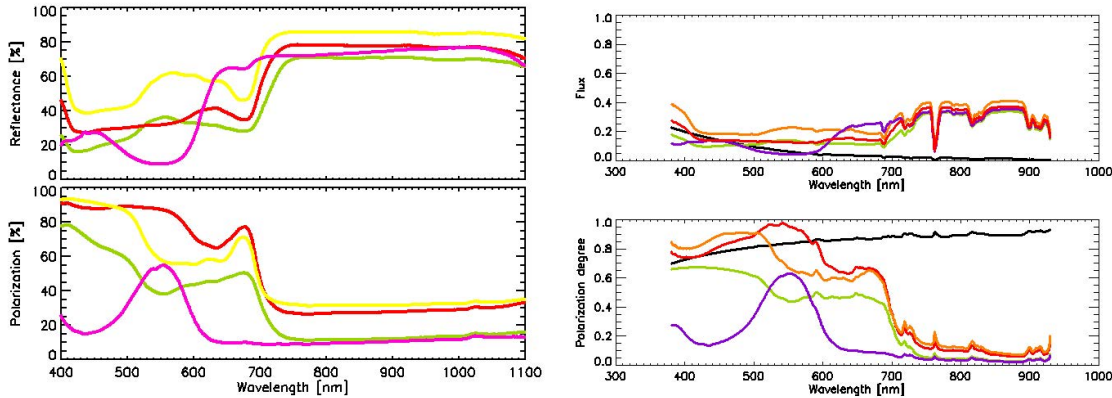


Figure 5: *Left*: Reflectance and linearly polarized spectra of plant samples containing various assemblies of biopigments: chlorophyll (green), anthocyanins (red), carotenoids (yellow), phycobiliproteins (purple) [25]. Note that the higher polarization occurs at the wavelengths where these biopigments most efficiently absorb photons. The so-called red edge near 700 nm is clearly visible. Also, polarization and reflectance are elevated if the surface of the plant is glossy (wavelength independent), cf., in the red and yellow samples. *Right*: Modelled reflectance spectra (top) and linear polarization degree spectra (bottom) for planets with the Earth-like atmosphere, 80% surface coverage by either of the four pigmented organisms shown on the left and 20% ocean surface coverage (visible hemisphere only). The high linear polarization degree clearly distinguishes the presence of the biopigments in contrast to the flux spectra. Black curve represents a planet with an ocean only [27]. The glint from its surface is highly polarized.

Present and near future observations of Earth-like planets around distant stars cannot resolve the planet surface and image its structures directly. However, uneven distribution of land masses and their various surface properties as on Earth seen from space produce rotational modulation of the reflected light which can be detected and used to constrain the overall surface coverage of various components which can be distinguished with flux and polarization measurements at different wavelengths. To calculate the biosignature effect we add surface below the atmosphere which implies new lower boundary conditions in Eq. (3). We allow the planetary surface to contain patches due to the presence of photosynthetic organisms, minerals, sands and water and include also scattering and absorption in the planetary atmosphere and clouds. The Earth atmosphere, ocean and clouds are the same as in [27]. Examples are shown in Fig. 5.

The presence of clouds masking the surface dilutes the information on the surface structure and composition. A completely cloudy atmosphere will obviously disguise the presence of biopigments (and everything else) on the planet surface. A small cloud coverage of around 20% will only marginally reduce polarization effect (see [25]). Thus, clouds are the most disturbing factor in detecting surface biosignatures, but weather variability should assist in successful detection if a planet is monitored long enough to reveal long-lived features on the surface.

The effect of the water ocean is also interesting [25]. The optical thickness of the ocean is basically infinite, so its surface is dark in most colours except for the blue, where it reflects the blue light scattered in the atmosphere. However, there is a bright glint at the subsolar location, which moves around the globe as the planet rotates. This glint is due to specular reflection and is highly polarized and practically white. Hence, an ocean only, cloud-free planet with an Earth-like atmosphere will appear somewhat blue (due to Rayleigh scattering in the atmosphere) and highly polarized. It seems therefore that the presence of an

ocean and optically thin atmosphere is most favourable for remote polarimetric detection of exoplanets and biopigments.

To conclude, we have presented a broad range of interesting examples where spectropolarimetry provides novel insights into physics of exoplanets and life. The theoretical components outlined in this paper have been developed since the 1950s, and they were successfully employed for probing atmospheres of the Earth, Sun, solar system planets, and other stars. It is imperative now to make a full use of these techniques for advancing our understanding of exoplanets and for searching for life in the universe.

This work was supported by the European Research Council Advanced Grant HotMol (ERC-2011-AdG 291659). The author was fortunate to have studied at the Saint Petersburg University under the guidance of Acad. Prof. V.V. Sobolev and the professors and docents of his faculty. The joint work in the group of Prof. Jan Stenflo at ETH Zurich was also a great benefit for this research.

## References

1. *V.V. Sobolev*, Radiative Transfer in Stellar and Planetary Atmospheres, Moscow, 1956.
2. *S. Chandrasekhar*, Radiative Transfer, New York: Dover, 1960.
3. *D.I. Nagirner*, JQSRT, this volume, 2016.
4. *D.M. Fluri, S.V. Berdyugina*, A&A, **512**, A59, 2010.
5. *J.E. Hansen, L.D. Travis*, Space Sci. Rev., **16**, 527, 1974.
6. *S.V. Berdyugina, S.K. Solanki, C. Frutiger*, A&A, **412**, 513, 2003.
7. *N.M. Kostogryz, S.V. Berdyugina*, A&A, **575**, A89, 2015.
8. *N.M. Kostogryz, I. Milic, S.V. Berdyugina, P.H. Hauschildt*, A&A, **586**, A87, 2016.
9. *N.M. Kostogryz, T.M. Yakobchuk, S.V. Berdyugina*, ApJ, **806**, 97, 2015.
10. *F. Allard, P.H. Hauschildt, D.R. Alexander, A. Tamanai, A. Schweitzer*, ApJ, **556**, 357, 2001.
11. *S. Witte, C. Helling, P. Hauschildt*, A&A, **506**, 1367, 2009.
12. *S.V. Berdyugina, A.V. Berdyugin, D.M. Fluri, V. Piirola*, ApJ Lett., **673**, L83, 2008.
13. *S.V. Berdyugina, A.V. Berdyugin, D.M. Fluri, V. Piirola*, ApJ Lett., **728**, L6, 2011.
14. *S.V. Berdyugina*, in Solar Polarization 6, eds. J.R. Kuhn et al., ASP Conf. Ser., **437**, 219, 2011.
15. *J.E. Hansen, J.W. Hovenier*, J. Atmos. Sci., **31**, 1137, 1971.
16. *H.C. van de Hulst*, Light Scattering by Small Particles, New York, Wiley, 1957.
17. *S.V. Berdyugina, C. Frutiger, S.K. Solanki*, A&A, **412**, 513, 2003.
18. *S.V. Berdyugina, J.O. Stenflo, A. Gandorfer*, A&A, **388**, 1062, 2002.
19. *N. Afram, S.V. Berdyugina*, A&A, submitted, 2016.
20. *L. Kreidberg, J.L. Bean, J.-M. Désert, et al.*, Nature, **505**, 69, 2014.
21. *F. Joos, H.M. Schmid*, A&A, **463**, 1201, 2007.

22. *J.O. Stenflo*, Solar Magnetic Fields, Kluwer, Dordrecht, 1994.
23. *N.Y. Kiang, J. Siefert, Govindjee, R.E. Blankenship*, *Astrobiol.*, 7, 222, 2007a.
24. *N.Y. Kiang, A. Segura, G. Tinetti, Govindjee, R.E. Blankenship, M. Cohen, J. Siefert, D. Crisp, D., V.S. Measows*, *Astrobiol.*, 7, 252, 2007b.
25. *S.V. Berdyugina, J.R. Kuhn, D.M. Harrington, T. Santl-Temkiv, E.J. Messersmith*, *Int. J. Astrobiol.*, 15, 45, 2016.
26. *G.D. Scholes, G.R. Fleming, A. Olaya-Castro, R. van Grondelle*, *Nature Chem.* 3, 763, 2011.
27. *D.M. Stam*, *A&A*, 482, 989, 2008.